Indian Journal of Geo Marine Sciences
Vol. 51 (10), October 2022, pp. 878-890
DOI: 10.56042/ijms.v51i11.3504

New insight in the determination of thermodynamic equilibrium thickness using heat budget over Barents Sea

D V Panicker[a], B Vachharajani*[,b], R Srivastava[a] & S R Oza[c]

[a]Department of Physics, School of Energy Technology, Pandit Deendayal Energy University, Gandhinagar, Gujarat – 382 426, India
[b]Department of Mathematics, School of Technology, Pandit Deendayal Energy University, Gandhinagar, Gujarat – 382 426, India
[c]Space Applications Centre, ISRO, Ahmedabad, Gujarat – 380 015, India
*[E-mail: bhasha.vachharajani@sot.pdpu.ac.in]

Received 01 September 2022; revised 7 November 2022

This paper examines various atmospheric and sea ice data to understand the Barents Sea's small-scale energy balance. The ERA-5 reanalysis products are used to calculate the atmospheric budget. Seasonal cycles detected using ocean-atmosphere interactions show that potential energy is substantially higher than kinetic energy over the Barents Sea, which is one of the reasons for it being colder than other places. The month of June experiences maximum radiation at the top of the atmosphere with a value of 16.19 Wm^{-2} and December experiences minimum with a value of 0.11 Wm^{-2}. However, the heat flow at the surface is the highest during December with values ranging between 0.64 Wm^{-2} and 0.69 Wm^{-2}. The system is constrained by declining solar flux, increasing heat flux at the Earth's surface, and atmospheric transport. Sea ice minimum and maximum months in the Barents Sea exactly coincide with those of the Arctic Sea. However, Barents Sea ice thickness is only limited to 3.5 m, but for the Arctic it is seen extending up to 4.5 m. Additionally, the area has recently experienced a massive exchange of heat (energy) between the ocean and the atmosphere, which is believed to be due to Atlantification, which is a well-known process. The Barents Sea is the region where the process of Atlantification is first observed. A new method has been developed to estimate the Thermodynamic Equilibrium Thickness (TET) of the sea. TET is calculated using a thresholding technique that is applied to total thermal radiation. The approach adopted for TET extraction is important as it generates several important fluxes, including the energy flux between the ocean surface and the atmosphere above it.

[**Keywords:** Barents Sea, Oceanic Energy, Sea Ice Thickness, Thermodynamic Equilibrium Thickness, Top Net Thermal Radiation]

Introduction

From decades of analyses, it is now known that the climate system is extremely complex in the way it interacts with other systems. The Earth's atmospheric system is mostly influenced by the cryosphere, the water bodies (oceans), the land surface, and the living beings. All the other spheres of the Earth are found directly interacting with the air above (atmosphere)[1,2]. One such influential phenomenon is the rapid melting of the sea ice over the Arctic, which is due to the recent increase in global temperatures. Such warming over the poles, also known as polar amplification[3,4], is one of the most recent noticeable climatic shifts. Growth and melting are two processes that are thought to sustainably convey heat in the polar directions, where it is subsequently exchanged between the ocean and atmosphere. Such transport symbolizes the requirement for an energy balance when the system undergoes an imbalance[5]. Therefore, studying the energy budget over the area gives an essential understanding of the pronounced warming and its trends[4]. According to previous studies, the Arctic energy imbalance at north of 70° N latitude between 2001 and 2015 is about 1 Wm^{-2}, similar to the world's imbalance average[6,7].

Due to the location of the area and being inaccessible, the majority of the time (due to the presence of thick sea ice), researchers highly rely on the data received from the satellites rather than those other real-time *in-situ* measurements[8-12]. The satellite data has further helped researchers identify that the Barents Sea, over the Arctic, has experienced a yearly Sea Ice Area (SIA) decline of almost 50 % over 1998 – 2008[(ref. 13)]. Such a significant decline was not only observed in summer season but was also prevalent during all four seasons (including winter)[14,15]. On a longer time scale, it is believed that the combination of enhanced advection and higher warmth of Atlantic water is what is responsible for the decrease in Barents Sea Ice Extent (SIE). The Atlantification process is

further accelerated by the advection of these waters into the Barents Sea[16]. During the inflow of Atlantic waters into the Barents Sea, it was discovered that the salinity of these waters varied from decade to decade[17], which makes it difficult for the scientific community to understand long-term trends and natural variability. Apart from salinity, the temperature of the Atlantic waters gushing into the Barents Sea also varies on multi-decadal time scales[17]; further making the distinction between long-term trends and natural variability more challenging.

In the current paper, reanalysis products and satellite datasets are being used to estimate the recent monthly mean and yearly averages to understand the balance of energy and heat between the atmosphere and the ocean (including the crysophere) over the Barents Sea. The current study focuses on solving two overarching objectives. Firstly, to investigate the prevailing atmospheric-ocean conditions of the Barents Sea. The sea which was known to be static previously has now seen tremendous fluctuations. North flowing ocean currents transport warm waters into the Barents Sea. These warm Atlantic waters that are drained into the Barents Sea prevent the formation of the surface sea ice and are also in turn melting the existing sea ice below. Therefore, it becomes vital in understanding the thickness of sea ice prevailing over the region. Secondly, the study tries to estimate the value of thermodynamic equilibrium thickness of sea ice considering the recent changes occurring over the sea. As possible, the obtained values are compared to observation-based/remote sensing products to determine their quality and consistency. This comparison will show how far the research has come since previous investigations. The key advance of this study is the development of a unique technique for connecting the heat budget of the system in assessing the equilibrium condition of the cryospheric state.

Materials and Methods

Framework: Heat budget, datasets, and methodology

Taking into account the scientific research of Trenberth[18] and Nakamura & Oort[19] the energy budget over the Barents Sea is derived. Atmosphere has energy budget starting at the ocean surface and extending to the top of the atmosphere, and is defined as:

$$\frac{\partial A_E}{\partial t} = -\nabla \cdot \overrightarrow{F_A} + R_{top} + F_{sfc} \quad \dots (1)$$

Here '∂t' is the time change in atmospheric energy storage; 'A_E' is the column representing the sum of the convergence of (i) atmospheric energy transport ($-\nabla \cdot \overrightarrow{F_A}$), (ii) the net radiation (R_{top}) at the top of the atmosphere, and (iii) the net heat flux (F_{sfc}) at the surface of the Earth. The convergence of atmospheric energy transport ($-\nabla \cdot \overrightarrow{F_A}$) denoted in Eq. (1) is represented as:

$$-\nabla \cdot \overrightarrow{F_A} = -\nabla \cdot \frac{1}{g}\int_0^{ps}\left(c_pT + \emptyset + Lq + k\right)\vec{v}dp \quad \dots (2)$$

In eq. (2), 'g' is the gravitational acceleration, (($c_pT + \emptyset + L_q$) is the dry static energy. 'c_p' is the specific heat of the atmosphere at constant pressure, 'T' is the temperature, '$\emptyset$' is the surface geopotential, 'L' is the latent heat of evaporation, 'q' is the specific humidity, 'k' is the kinetic energy, '$\vec{v}$ ' is the horizontal wind vector, and 'p' is the pressure. Further, the net heat flux at the Earth's surface (F_{sfc}) referenced in eq. (1) is addressed as:

$$F_{sfc} = R_{sfc} + H + E \quad \dots (3)$$

Where, 'R_{sfc}' is the net radiation at the surface, 'H' is the turbulent sensible flux, and 'E' is the latent heat flux.

The energy budget of the subsurface column, if characterized by water is represented as:

$$\frac{\partial O_E}{\partial t} = -\nabla \cdot \overrightarrow{F_O} + \nabla \cdot \vec{F_i} - F_{sfc} \quad \dots (4)$$

Where, 'O_E' is oceanic energy storage, '$\overrightarrow{F_O}$' is the horizontal convergence of the oceanic sensible heat flux, '$\vec{F_i}$' is the horizontal divergence of the latent heat flux of sea ice, and 'F_{sfc}' is the net heat flux at the Earth's surface as explained in Eq. (1).

'F_i ' in Eq. (4) denotes heat exchanges related to the separation of sea ice by winds and currents over the sea. Some of the variables, like the sensible heat of the ice transport, kinetic energy, and sensible heat transport, are not considered in the equation. The kinetic energy here is obtained from the shift of sea ice along the shoreline of the sea. Further, sensible heat transfer occurs due to the transport of water from the sea to the ocean or vice versa. Hence Eq. (4) can be rewritten as:

$$\frac{\partial O_E}{\partial t} = -\nabla \cdot \overrightarrow{F_O} - F_{sfc} \quad \dots (5)$$

Top net thermal radiation, addressed as '*ttr*' is otherwise called terrestrial or Outgoing Long wave Radiation (OLR) transmitted to space at the top of the atmosphere.

$$ttr = -OLR \quad \ldots (6)$$

Top net solar radiation represented as '*tsr*' is defined as the difference between the incoming solar radiation and that reflected by the Earth's atmosphere, *i.e.*

$$tsr = ISR - OLR \quad \ldots (7)$$

Data sources

Atmospheric reanalyses

To understand the ocean heat conditions; temperature[20], geopotential height[20], specific humidity[21], kinetic energy[21], V-wind[21], pressure[20], net radiation at the top of the atmosphere[20], net heat flux at the Earth's surface[20], top net thermal radiation (ttr)[20], and top net solar radiation (tsr)[20] datasets were extracted from ERA-5 reanalysis with a spatial resolution of 0.25°×0.25°, visit: https://cds.climate.copernicus.eu. The incoming solar radiation from the Sun is known as net radiation at the top of the atmosphere. It refers to the amount of radiation that is transmitted over a horizontal plane. The amount of heat transferred from the Earth's surface to the atmosphere as a result of turbulent air movement, excluding any heat transfer carried on by condensation or evaporation, is known as net heat flux at the Earth's surface. The temperature gap between the surface and the surrounding atmosphere determines the extent of the sensible heat flow. Convection is positive if the surface is warmer than the atmosphere, otherwise, it is negative. Ocean heat content data[22] is retrieved from the World Ocean Database of the National Oceanic and Atmospheric Administration/National Center for Environmental Information (NOAA/NCEI), with a spatial resolution of 1°×1°. All the aforementioned datasets were extracted for Barents Sea for the span of 2002 – 2020. The accuracies of these datasets are mentioned in Table 1.

Sea ice data

SIA, SIE and SIT monthly datasets from CryoSat-2 and Envisat for the periods 2002 – 2010 and 2010 – 2020, respectively are used to estimate Barents Sea ice conditions[23]. All datasets (SIA, SIE and SIT) have a spatial resolution of 0.25°×0.25°. SIT error is estimated to be between 0.04 – 0.06 m[(refs. 24,25)]. The accuracies of these cryospheric datasets are mentioned in Table 2.

Table 1 — Validation of atmospheric variables with their R, biases and RMSE

Variable	Retrieved from	Validation with *	R	Bias	RMSE
Temperature (K)	ERA-5	N-ICE2015[(ref. 30)]	0.96	+3.40	5.30
		DAMOCLES[(ref. 31)]	0.74	+0.51	2.61
Specific humidity (kg kg^{-1})		N-ICE 2015[(ref. 30)]	0.98	0.00	0.50
		DAMOCLES[(ref. 31)]	0.56	+0.40	0.75
V-wind (ms^{-1})		N-ICE 2015[(ref. 30)]	0.92	+0.40	1.40
		DAMOCLES[(ref. 31)]	0.71	+0.43	1.80
Pressure (hPa)		RAOBCORE[(ref. 32)]	N. A	+1.66	N. A
Net radiation at the top of the atmosphere (Wm^{-2})		CERES and CAVE[(ref. 33)]	0.94	-18.52	26.95
Net heat flux at the Earth's surface (Wm^{-2})		N-ICE 2015[(ref. 30)]	0.32	-14.00	32.00
Top net thermal radiation (Wm^{-2})		MERRA – 2[(ref. 34)]	0.70	+5.00	N. A
Top net solar radiation (Wm^{-2})		NIBIO - CMP11 or CMP13 pyranometers[(ref. 35)]	0.99	+4.10	10.20
Ocean heat content (J)	NOAA	In-situ observation (2006 - 2015)[(ref. 36)]	N. A	±0.10	0.61
		CERES EBAF EEI[(ref. 37)]	0.44	N. A	0.40

*N-ICE2015 - Norwegian Young Sea-ice cruise, DAMOCLES - Developing Arctic Modeling and Observing Capabilities for Long-term Environmental Studies, RAOBCORE - RAdiosone OBservation COrrection using Reanalyses, CERES - Clouds and the Earth's Radiant Energy System, CAVE - *CERES* ARM Validation Experiment, MERRA - Modern Era Retrospective-Analysis for Research and Applications, NIBIO - Norwegian Institute of Bioeconomy Research, CMP11 or CMP13 - Kyoto Protocol, EBAF - Energy Balanced and Filled, and EEI - Earth's energy imbalance

Table 2 — Validation of sea ice parameters with their R, biases and RMSE

Variable	Retrieved from	Validation with *	R	Bias	RMSE
Sea ice Area (km^2)	CryoSat-2 and Envisat	DMSP-F8 SSM/I [(ref. 37)]	0.99	0.07×10^6	0.05×10^6
Sea ice Extent (km^2)		DMSP-F8 SSM/I [(ref. 37)]	0.99	0.05×10^6	0.09×10^6
Sea ice Thickness (m)		ICESat[(ref. 38)]	N. A	0.14-0.51	0.04-0.06

*DMSP - Defense Meteorological Satellite Program -F8, -F11 and -F13, SSM/Is - Special Sensor Microwave/Imagers (SSM/Is), and the DMSP-F17 Special Sensor Microwave Imager/Sounder (SSMIS), and *ICESat* - Ice, Cloud and land Elevation Satellite

Methodology

Atmospheric-ocean energy budget: Annual cycle

Various atmospheric reanalyses variables are investigated during the period 2002 – 2020 to understand the energy interaction of the ocean with the atmosphere. These data are extracted from ERA-Interim reanalysis over the Arctic Cap. Later using a shape file the Barents Sea is extracted. Thereafter, the mean monthly, seasonal product for each of these parameters were taken out and plotted for the region as depicted in Figure 1. These parameters are brought to a uniform resolution of 25 km (by interpolation/ extrapolation).

Estimation of Thermodynamic Equilibrium Thickness (TET)

In this study, a technique has been developed on the sea ice over the Arctic region such that one can know the value of TET during different temporal (different months of the year) and spatial domains (different seas of the region). This has been attained by changing the threshold values of the varying parameters. The first step in TET detection is to determine thresholds for *ttr*. Although the only fact known to date is that, when the ice thickness reaches a point where no exchange of heat takes place from the water, the ice stops developing and is considered to have reached thermodynamic equilibrium. However, it was understood that the threshold value for *ttr* changes for each sea over the Arctic region due to its topographical/oceanic features. Here an attempt has been made to identify a suitable threshold for the Barents Sea by noting the number of pixels having the least *ttr* values. The threshold value of *ttr* is estimated, which is made to run across all the pixels covering the sea. By overlaying *ttr* with SIT spatial plots, it was understood that the maximum thickness was shown by sea ice when the *ttr* value was less than -7 Wm^{-2}. Therefore, after performing such sets of methods, it was determined that the *ttr* threshold value over the Barents Sea is -7 Wm^{-2} for the years 2002 – 2020.

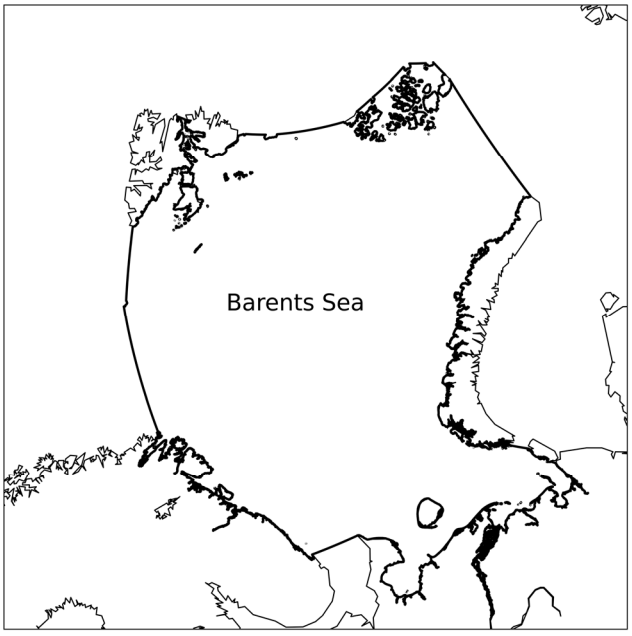

Fig. 1 — Barents Sea (60 – 85° N, 10 – 70° E)

The second step is to apply a boundary limit to SIT to determine its growth. For every month, 0.05, 0.25, 0.50, 0.75, 1.0, and 2.0 m of spatially homogeneous SIT growth[26] were fixed, with finer runs of 0.05 m. The mean value of SIT over Barents Sea during the specified time range is found to be 2.0 m. SIT less than 1.0 m is categorized as sensitive SIT, where further thinning is possible. Over the Barents Sea, the lowest value of SIT obtained is 0.05 m; which shows the presence of open waters. Considering all these conditions, SIT was bounded to the condition that it can grow/melt up to 0.5 m from the existing state.

Results and Discussion

Ocean-atmosphere conditions of Barents Sea

Table 3 gives monthly averages and annual means of the basic atmospheric budget terms (Eq. (2)) over the Barents Sea. C_PT which denotes the internal energy is seen to display normal distribution behaviour. From the values represented in Table 1, it is evident that maximum internal energy over Barents is obtained for June (28.08×10^4 Jkg^{-1}) and minimum during November (24.18×104 Jkg^{-1}) during the span of 2002 – 2020. Similarly, potential energy is also seen to exhibit a Gaussian distribution with the highest value lying between June – August (highest in July with a value of 48.84×10^4 m^2s^{-2}) and the lowest during November – December (42×10^4 m^2s^{-2}). Therefore, the pattern demonstrates that internal and potential energy jointly overlaps each other for the span of 18 years. Unlike C_PT and Lq in eq. (2), which is the product of latent heat of evaporation (L) and specific humidity (q), does not exhibit any symmetry. Lq (latent energy) reaches a peak between August and October, with values up to 10 Jkg^{-1}, followed by values around 9 Jkg^{-1} in other months. Kinetic energy (k) is often neglected (for the fact that the term is quite small) while considering atmospheric transport and storage. However, it is included in this work since this energy behaves in a completely different way from the other dominating energies. The minimum value of k is observed in the month of June – July

Table 3 — Monthly and yearly averages of the atmospheric energy budget of Barents Sea calculated for the span of 2002 – 2020

Months	C_pT (x10^4) (Specific Heat and Temperature)	$\emptyset$ (×10^4) (Surface Geopotential)	Lq (Latent heat of evaporation and Specific humidity)	K (Kinetic Energy)	$-\nabla \cdot F_A$ (Convergence of atmosphere energy transport)	R_{top} (Net radiation at the top of atmosphere)	F_{sfc} (Net radiation at the top of atmosphere)	$\frac{\partial A_E}{\partial t}$ (Change in atmosphere energy storage with time)
Jan	25.39	44.05	09.60	0.62	107.08	00.23	-0.69	106.62
Feb	24.71	44.09	09.57	0.60	111.45	01.07	-0.65	111.87
Mar	25.77	44.84	09.48	0.60	111.32	03.80	-0.64	114.49
Apr	26.97	46.51	09.82	0.50	90.87	08.76	-0.54	099.08
May	27.64	47.86	09.94	0.39	66.51	13.77	-0.54	079.74
Jun	28.08	48.73	09.97	0.34	89.19	16.19	-0.45	104.93
Jul	27.98	48.84	09.96	0.33	93.98	14.92	-0.35	108.56
Aug	27.32	48.02	10.02	0.34	98.01	10.53	-0.23	108.32
Sep	26.03	46.34	10.15	0.44	105.99	05.34	-0.14	111.20
Oct	24.91	44.46	10.18	0.51	113.86	01.76	-0.38	115.24
Nov	24.18	42.97	09.61	0.57	105.54	00.39	-0.59	105.34
Dec	25.18	42.90	09.25	0.60	111.25	00.11	-0.64	110.72

(0.33 – 0.34 Wm^{-2}) and the maximum during January (0.62 Wm^{-2}). It is usually known that when potential energy falls, kinetic energy increases, according to the rules of physics that govern the atmosphere. In this case, potential energy is greater than kinetic energy. This is also one of the reasons for the Arctic to be so cold compared to other regions. Internal energy, which is the sum of potential energy and kinetic energy, is excessively inclined to the patterns followed by potential energy as its values are considerably high. The convergence of atmospheric heat transference $-\nabla \cdot F_A$ (which is also the integral sum of all the energies mentioned above), also exhibits a symmetric/cyclic behaviour. It peaks down to a value of 66.51 Wm^{-2} during May. The highest value is 113.86 Wm^{-2} found during October. The maximum R_{top} (16.19 Wm^{-2}) is in June, and the lowest is in December (0.11 Wm^{-2}). When the seasons of the Barents Sea are classified as winter, spring, summer, and autumn, the values of R_{top} anywhere in the Arctic is at its highest in the summer and at its lowest in the winter. Winter includes the months of December, January, and February, whereas spring includes March, April, and May. Further, summer contains the months June, July, and August, and lastly, autumn consists of September, October, and November months. However, F_{sfc} is seen to be highest in December (0.64 – 0.69 Wm^{-2}). While observing the spatial variation, it is understood that larger pixel values of F_{sfc} were visible over open waters. These smaller open areas enable solar heating; replenishing the ocean's sensible heat and allowing ice to melt rapidly even during the winters. The system is constrained by declining solar flux (R_{top}), as well as

Table 4 — Monthly cycle of O_E, ttr and tsr of Barents Sea

Months	O_E(×10^8)	ttr	tsr
Jan	1.06	-6.09	0.11
Feb	0.98	-6.15	0.52
Mar	0.35	-6.24	1.90
Apr	0.05	-6.64	4.42
May	0.72	-7.14	7.37
Jun	1.72	-7.52	9.20
Jul	2.79	-7.74	8.58
Aug	3.88	-7.53	5.81
Sep	4.26	-7.14	2.87
Oct	3.57	-6.68	0.92
Nov	2.93	-6.31	0.18
Dec	1.98	-6.14	0.05

increase in both F_{sfc} and atmospheric transport. In general R_{top} and F_{sfc} help in providing atmosphere-only and surface-only variabilities over Barents Sea. $\partial A_E / \partial t$, is the sum of $-\nabla \cdot F_A$, R_{top} and F_{sfc} behaves closer to $-\nabla \cdot F_A$ as it contributes ~90 % to the total energy. Overall the balance between the radiant energy that reaches the sea from the sun and the energy that travels back out to space is depicted in Table 3.

The summer months of June and July experience the largest increase in oceanic sensible heat, whereas November and December see the highest decline (Table 4). The melting of sea ice occurs between June and August, with the highest amount melting in July, which is roughly double the sensible heat gain, as shown in Figure 2. This melting primarily occurs in areas of open water. The most healthy ice growth is seen in September and October, tailed by a decrease from November to December and then a second

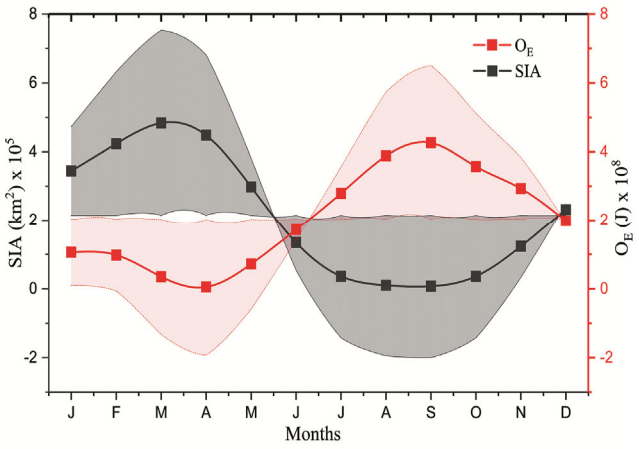

Fig. 2 — Climatology of Sea Ice Area (SIA) and Oceanic Energy (O_E) over Barents Sea for the span 2002 – 2020

highest in January and February. In autumn, the topmost peak is attributed by the presence of abundant open water that allows for new ice growth. While one might expect a decline in ice growth during winter following the October peak, or a relatively constant growth. The second peak acknowledges that the air temperatures reach their minimum in January and so forth the production of fresh, thin ice continues along the Barents Sea opening where offshore ice movement creates many leads, resulting in new ice formation. The monthly cycle in oceanic sensible heat storage (from Fig. 2) appears to be very dominant in the Barents Sea. Seasonal variations in sensible heat storage over the region are far greater than expected. However, the oceanic heat advection near this sea's opening delays the autumn cooling of the column of the Barents Sea to meet the Atlantic branch. The ocean circulation continues to transport heat into this region even when the water at the surface cools. This adjustment explains why the sensible heat content in November is so high. Between November and December, the water column cools dramatically. However, until January and February, sufficient heat is present to curtail ice development.

Comparing with other seas in the Arctic region, the Barents Sea experiences the most considerable amount of heat, *i.e.*, the sensible heat stored over the sea is the highest compared to any other sea present at the Arctic location. Additionally, the seasonal variations in this energy over the sea (the Barents Sea) are found to be increasing with respect to time. The Barents Sea area is known for its intense autumn and winter freezing, as well as its significant summer warming at the uppermost layer of the ocean which is due to the net surface flux. Nevertheless, the freezing of the water column in this area is postponed during autumn because of the oceanic energy transport through the Barents Sea opening (branch of the Barents Sea - Atlantic inflow). Considering that the surface waters drops in temperature, the oceanic circulation systems continues to transport energy in the form of heat into this area, resulting in a compensation effect that explains the relatively elevated sensible energy content in November. Even though the water column cools off significantly between November and December, there is sufficient amount of stored heat to restrict the growth of ice till January and February.

Maps representing the net surface flux for four midseason months (January, April, July, and October) indicate the significance of the Barents Sea in the overall climate changes over the Arctic (Fig. 3). During January (Fig. 3a), the fluxes over ocean areas are upward, but their magnitude is smaller, while the fluxes over land regions are downward. In April (Fig. 3b), strong rising fluxes are noticeable over open ocean areas, containing regions around Svalbard where significant thermal contrast between air and sea, exist. Over the ocean covered by ice, there are minor upward fluxes, while over land areas the upward fluxes are even more minimal. In July (Fig. 3c), fluxes are upward all over, major over ocean areas south of 72° N where strong ice melt and ice free zones cause rapid solar warming, displacing the ocean's sensible heat storage. This severe distinction during July, associated with other months, helps to comprehend that the highest amount of oceanic energy is confined during the summer months. Seas which have vast land boundaries frequently have Arctic frontal zones during summers due to these variations. This leads to positive environments for summer cyclogenesis, particularly along the coasts of eastern Eurasia and Alaska[27]. In October, the situation returns to winter conditions, as shown in Figure 3(a), with significant upward fluxes over exposed sea, regions in the north, where thick ice is forming, associated to lower fluxes over landlocked boundaries in the south, where the sea ice is thinner.

Sea ice conditions of Barents Sea

The monthly variations of the Barents Sea ice conditions provide important information for the examination of Arctic environment. Hence, investigating the Barents total sea ice availability is very crucial and essential to understand the impact of Arctic sea ice coverage on global climate alterations. The total sea ice measurements are determined every

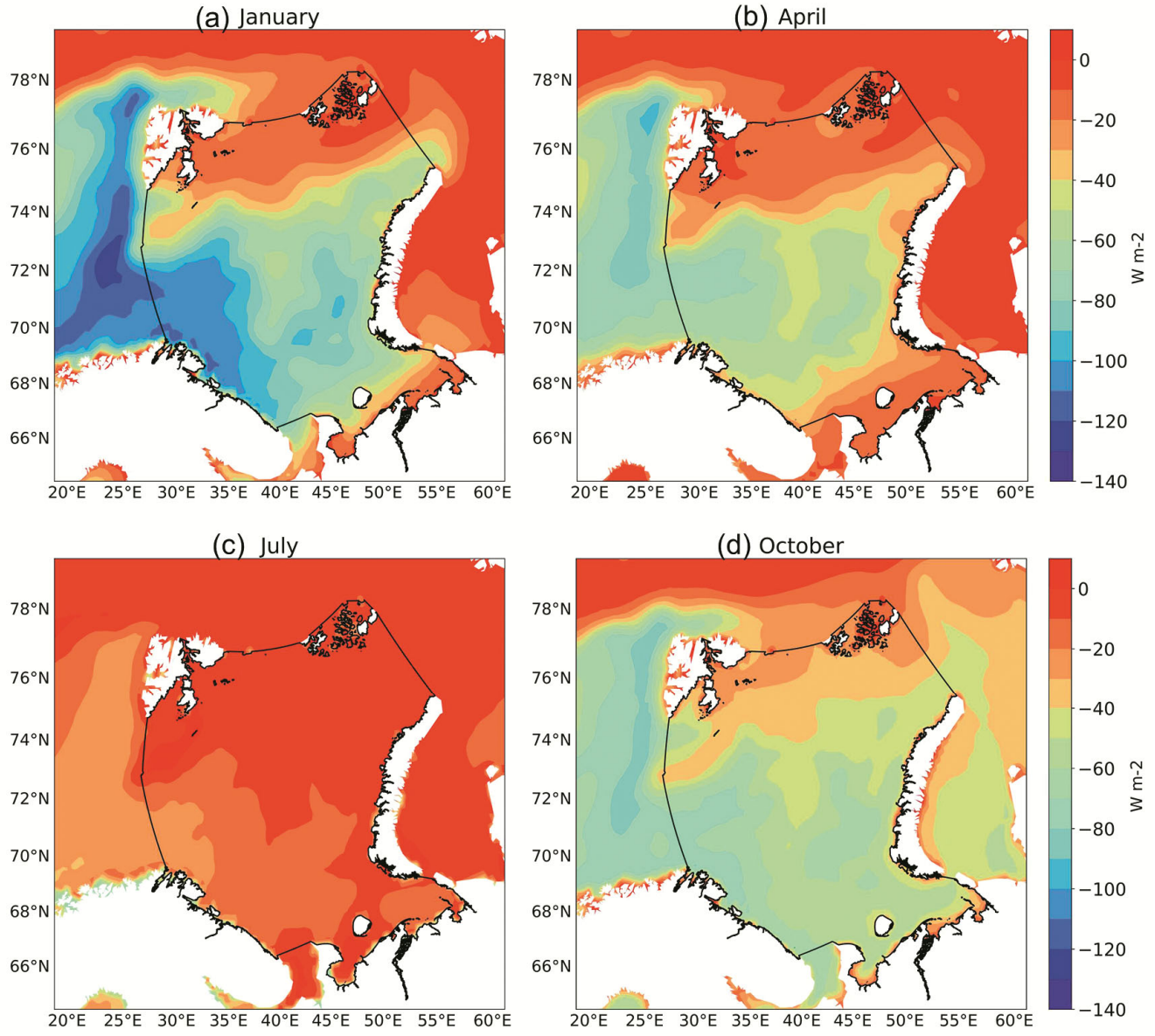

Fig. 3 — Spatial plots of net surface heat flux for (a) January, (b) April, (c) July, and (d) October over Barents Sea for the span of 2002 – 2020

month and aggregated into 18-year averages on an annual basis. The average SIA, SIE and SIT results for the span of 18 years was obtained and is presented in Table 5. Seasonally, the highest value of all the three parameters (SIA, SIE and SIT) is observed during spring, followed by winter, autumn and the summer. After spatial analysis of sea ice conditions in terms of SIA for each season from 2002 – 2020, it was discovered that there is a noticeable reduction in SIA during the winter months in the Barents Sea, with a yearly decrease of approximately 2 % (with a significant level of 95 %). This decline is attributed to the warmer northward flowing Atlantic water heating up the surface water, leading to a significant reduction in SIA. In the spring, the Barents Sea experiences a more significant reduction in their SIA trends compared to the winter months. In the autumn, the areas (pixels) where SIA trends are considerably decreasing become smaller and move toward the edges of the Arctic compared to the summer months[28]. However, their distribution is still more widespread than during the spring and winter seasons[29].

From January to April, the values of all three parameters in the monthly cycle are seen gradually increasing (Table 5). SIA increases by 30.23 %, SIE by 27.73 %, and SIT from 0.60 to 0.84 m. After April,

Table 5 — Monthly life cycle of sea-ice represented by SIA, SIE and SIT over Barents Sea

Months	SIA ($\times 10^5$)	SIE ($\times 10^5$)	SIT
Jan	3.44	5.12	0.60
Feb	4.23	6.14	0.70
Mar	4.84	6.86	0.83
Apr	4.48	6.54	0.84
May	2.98	4.73	-
Jun	1.34	2.56	-
Jul	0.36	0.81	-
Aug	0.10	0.26	-
Sep	0.07	0.17	-
Oct	0.36	0.72	-
Nov	1.24	2.00	0.34
Dec	2.31	3.59	0.42

the declining trend of sea ice is observed and reaches its maximum declination state in September. From November to December, further development in the sea ice conditions occurs which causes SIA to increase from 1.24×10^5 km^2 to 2.31×10^5 km^2, SIE from 2.00×10^5 km^2 to 3.59×10^5 km^2 and SIT from 0.34 to 0.42 m over the Barents Sea. The sea ice recovery over the winter has been declining, according to the monthly climatology shown in Table 5, suggesting that the sea ice is already fragile when the summer melting season arrives. One possible explanation for this phenomenon is that the underlying ocean is warmer.

Understanding the contribution of the Barents Sea to the Arctic area as a whole requires a comparison of this sea with the state of the sea ice (in this case, SIT). Figure 4 shows histogram of SIT over Arctic and

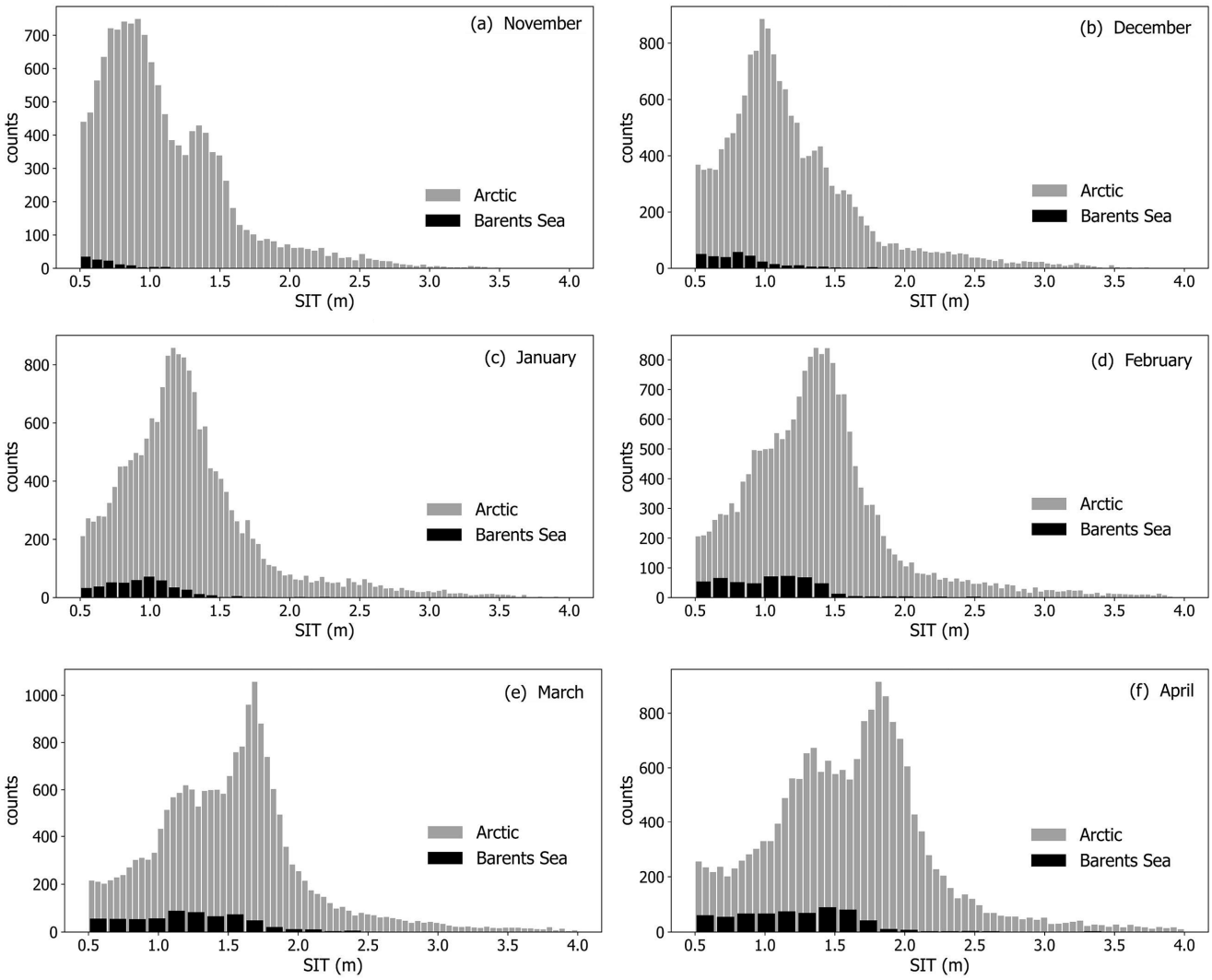

Fig. 4 — Histogram representing percentage contribution of Barents Sea Ice Thickness (SIT) over Arctic Sea Ice Thickness (SIT) during (a) November, (b) December, (c) January, (d) February, (e) March, and (f) April for the span of 2002 – 2020

Barents Sea for various months; from November to April. It is found from the plots that, the maximum number of pixels in which Arctic Ocean and Barents show presence of SIT are approximately 900 and 90, respectively. The range of SIT over the Arctic extends up to 4.50 m, but for the Barents Sea, it is limited to around 3.50 m, as the sea is a subset of the Arctic. As explained previously (in Table 4), it is understood that from November – December a gradual growth of SIT is observed till it reaches its maximum by March – April. During November (Fig. 4a), maximum value of SIT (> 30 counts) is found to have values 1.0 – 0.5 m over Barents. Moreover, these values are seen to display a step-wise behavior with ~35 counts for 0.5 m, ~25 counts for 0.6 m, ~10 counts for 0.8 m, and < 5 counts for 1 m. The Arctic as a whole shows a bimodal pattern with its first peak at SIT 0.8 m (700 counts) and second at 1.3 m (counts > 400). The contribution of Barents SIT to Arctic SIT is 11.71 % during this month. However, during December (Fig. 4b), the SIT count increases greater than 55 counts. The highest count is observed for SIT of 0.8 m. For Arctic, unlike in the previous case, the counts have ascended up to 800 and the first peak seems to be thicker with 1.0 m thickness. Further, the contribution of Barents to Arctic SIT has increased to 20.61 % during December. In January (Fig. 4c), Barents SIT is observed to follow a normal distribution curve with its maximum peak (70 counts) at 1.0 m. During this month the SIT is seen to extend more than 2 m. Similar is the pattern observed in the case of Arctic with its highest peak at 1.25 m. Here the influence of Barents SIT over Arctic region has further increased to 26.68 %. By February (Fig. 4d), all the thicknesses ranging between 0.5 – 1.4 m display a homogeneity over Barents. Yet, thickness > 1.4 m is seen to be present in scarce (having counts < 10). Additionally, over Arctic the SIT is seen to be extending to higher thickness > 3.0 m having counts ranging ~100. Due to the higher availability of thicker sea ice over Barents, the contribution of Barents SIT to Arctic SIT has increased reaching up to 29.33 %. Unlike February, in March (Fig. 4e) the count of Barents SIT reaches > 80. In this month, SIT > 3 m is seen to be visible for some (0 – 20) pixels. The plot now reveals that the existing sea ice has now thickened to reach greater SIT values. Similarly, Arctic also has higher availability of SIT (> 1000 counts). At this stage, SIT over Arctic reaches up to 4 m. Here, the contribution is about 35.64 % which is as expected. March is also the month in which the Arctic sea ice conditions are at its maximum attainment stage. By April (Fig. 4f), Barents Sea experiences sea ice loss causing higher SIT to lose its thickness resulting in only a smaller number of pixels having value greater than 2.0 m. Similarly, Arctic count also drops to 900, which ultimately causes reduction in the percentage contribution of Barents to Arctic *i.e.* 31.98 %.

Thermodynamic Equilibrium Thickness (TET) over Barents Sea

The change and variability of ocean-atmosphere conditions along with sea ice interactions are now understood over the Barents Sea. Based on the methodology adopted, TET is derived for November – April and the plots are displayed in Figure 5. As per the definition of National Snow and Ice Data Center (NSIDC), TET is the thickness at which ice no longer grows (assigned limit +0.50 m) because it is so thick that heat from the ocean (> -7 Wm^{-2}) can no longer be conducted through the ice. To better understand the range of TET, focus is primarily made on the atmospheric parameter; *ttr* in the Barents Sea. Table 2 shows the temporal variability of *ttr* over various months for years 2002 – 2020, which are significantly seen impacting the growth of sea ice. When examining the spatial data, it was observed that the area of open water in the northern Barents Sea expanded toward the north when the threshold temperature for ice formation was lower than -7 Wm^{-2}. With the perquisite knowledge about the existing life cycle of sea ice over Arctic, we found that in the case of Barents, a robust difference in the TET is observed. During November the TET over Barents is 1.44 m, after which it is seen to be gradually rising. SIT achieves TET of 1.94 m in December, 2.25 m in January, 2.51 m in February, and 2.96 m in March. The highest amongst all is the TET occurs during March. Finally, by April TET in accordance with SIT also reduces to 2.62 m. Overall, the life cycle of TET is exactly similar to SIT (as TET is the subset of SIT).

Estimating the TET of Arctic Sea ice holds significant advantages, particularly in the area of climate change research and its impacts on the Arctic region. Understanding TET offers an essential framework for estimating the extent and rate of ice loss as the Arctic undergoes major shifts as a result of climate change. Additionally, it helps us comprehend the delicate balance between ice formation and melting under changing climatic conditions. By combining equilibrium thickness calculations with

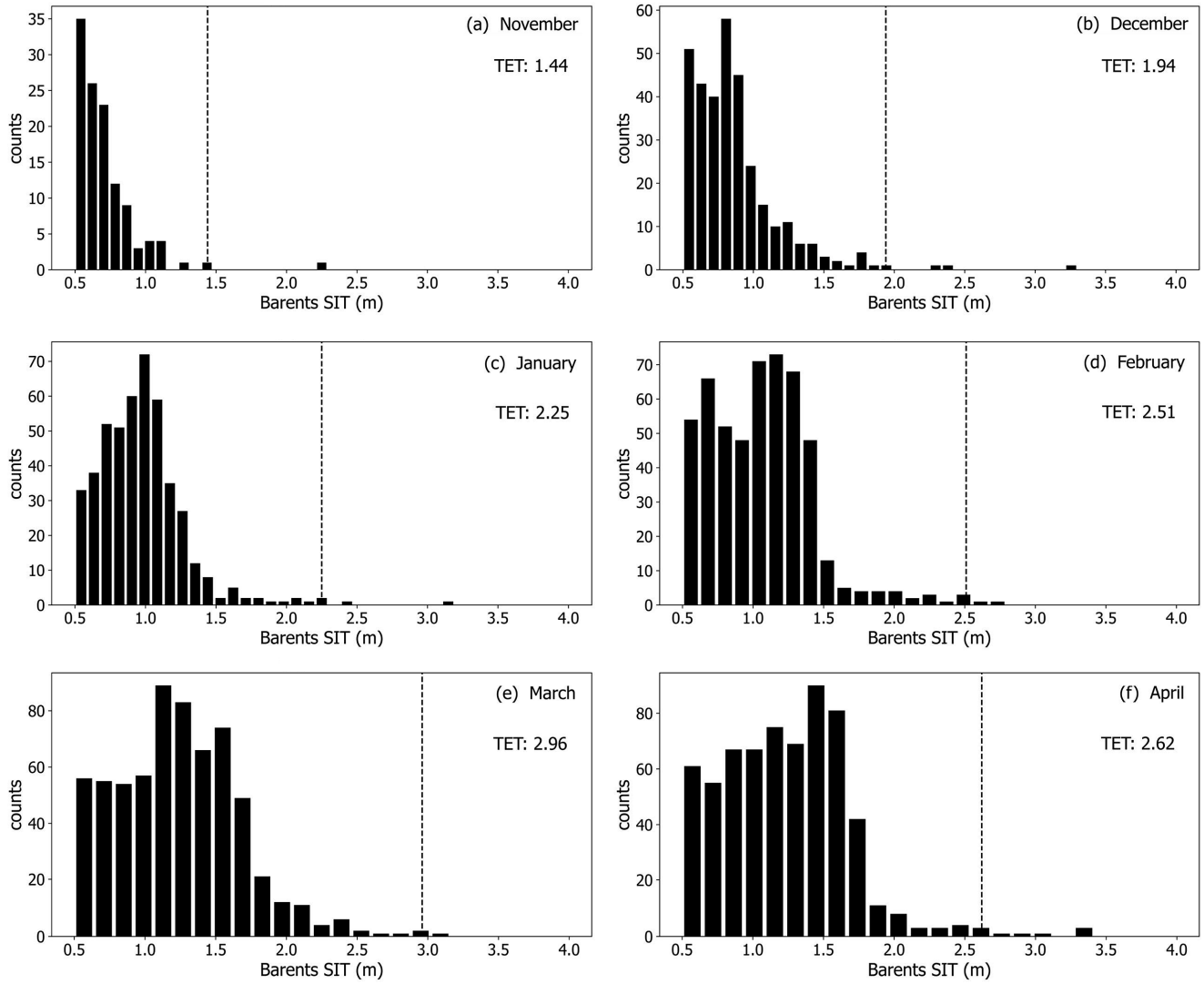

Fig. 5 — Retrieved Thermodynamic Equilibrium Thickness (TET) over Barents Sea during (a) November, (b) December, (c) January, (d) February, (e) March, and (f) April for the span of 2002 – 2020

measurements of ice extent, scientists can estimate the volume of Arctic Sea ice, providing valuable information on long-term trends and their implications for global sea levels and Arctic ecosystems. Also, based on this calculation, several models and simulations can be developed, aiding in predicting future changes in ice cover and guiding decision-making for climate change mitigation and adaptation strategies. Furthermore, TET is closely linked to ecosystem dynamics, influencing habitat availability for various species and enabling assessments of the impacts of diminishing ice cover on Arctic biodiversity. Additionally, the computation of TET plays a crucial role in assessing the feasibility and safety of shipping routes and resource exploration in the Arctic, guiding planning and risk assessment efforts. Finally, this parameter is fundamental for climate models and Earth system studies, enhancing our understanding of climate dynamics and facilitating more accurate climate projections at regional and global scales.

Conclusions

According to present study, the convergence of energy transport and net surface fluxes has a first-order impact on the atmospheric energy balance. From spring to summer, the overall amount of incoming solar radiation increases, giving the atmosphere more energy. The radiation further increases the amount of net flux in the atmosphere.

The seasons are also found to experience greater surface fluxes, which cause the sea ice to replenish and store more sensible heat. Such absorption of heat leads to further melting of the sea ice present in the region. Additionally, the atmospheric column above the Barents Sea entrance is affected by the oceanic heat that is pulled in via the opening by the mechanism of advection, thereby delaying autumn cooling. The Atlantic inflow which is warmer than the Arctic water certainly inhibits the growth of sea ice. The ocean circulation continues to bring heat into this region despite the fact that the surface waters remain frozen at this point. The replacement of cold waters with hot waters is the reason why November experiences high sensible heat content. By December, the water column begins to chill significantly, but the amount of heat stored in them doesn't adequately promote ice growth until January and February. The thickness of the sea ice at which there is no heat transmission between the two mediums may also be determined using *ttr*. The sea ice serves as a heat barrier between the ocean and the atmosphere.

While comparing the presence of Barents SIT with Arctic SIT, it was understood that the range of Barents SIT is only limited to 3.5 m, but for the Arctic as a whole; it is seen to extend up to 4.5 m. The basic reason behind it is the current process of Atlantification. During this process, waters from the Atlantic Ocean move into the Arctic Circle from the south, bringing warm and dense (more saline) waters into the region, which causes the existing sea ice to melt. The melting causes a reduction in sea ice coverage, leading to less reflection of sunlight back into space, which causes increased absorption of solar radiation by the ocean. The open waters further increase and the sea ice albedo further decreases, causing the water to absorb more heat from the space. This further warms the water and contributes to even more melting of sea ice, exacerbating the effects of Atlantification. As the process is first experienced over the Barents Sea; a new methodology for estimating the sea's Thermodynamic Equilibrium Thickness (TET) has been established. The life cycle of sea ice when considering the parameters SIA and SIE, was noted to reach its maximum state in March and minimum in September. Barents Sea plays a critical role in regulating the climate of the Arctic, contributing up to 36 % of Arctic Sea ice. With the growth of sea ice to its maximum attainment (by the month of March) it is seen that the percentage contribution of the sea over the ocean also increases gradually from 11.71 % (November) to 35.64 % (March), which is significantly large. The derivation of TET with the help of *ttr* also helps one understand the potential capacity of the sea to hold up its heat. With the shift in seasons from winter to summer, it is noted that the release in the thermal radiation from the ocean through the ice also varies (increases), causing variable TET for each month. The maximum obtained TET is during March (2.96 m) and the minimum in November (1.44 m).

The development of such an approach makes it easier to comprehend sea ice movement using TET. Last but not least, TET is useful in figuring out a number of important fluxes, such as the heat flux between the oceanic and atmospheric surfaces. In the case of the Barents Sea, due to the intertwined interactions between the sea and the atmosphere, extensive open water formed during the summers causes the air temperatures to be far more likely above average through autumn ultimately affecting winter sea ice formation. Further development of this technique by incorporating the external driving forces of sea ice-atmospheric and oceanic variables will help in accurately computing the thickness of sea ice at micro scale and macro scale. Further work may be done to apply this model to various seas of the Arctic to investigate its varying threshold along with the limitations of this methodology.

Acknowledgements

The authors are grateful to the National Oceanic and Atmospheric Administration/National Center for Environmental Information as well as CryoSat-2 and Envisat for making their datasets publicly available.

Conflict of Interest

The authors affirm that they do not have any competing interests.

Ethical Statement

This material is the authors' own original work, which has not been previously published elsewhere. The paper properly credits the meaningful contributions of co-authors.

Author Contributions

DVP: visualization, formulating methodology, software, data collection, and writing-creating the first draught; BV & RS: conceptualization, visualization, investigation and editing; and SRO: investigation and editing.

References

1 Snyder C W, Mastrandrea M D & Schneider S H, The Complex Dyanmics of the Climate System, *Philosophy of Complex Systems*, 10 (2011) 467-505. https://doi.org/10.1016/b978-0-444-52076-0.50017-1

2 IPCC, *Climate Change 2001: Synthesis Report*, A Contribution of Working Groups I, II, and III to the Third Assessment Report of the Integovernmental Panel on Climate Change, edited by Watson R T & the Core Writing Team, (Cambridge University Press, Cambridge, United Kingdom, and New York, NY, USA), 2001, pp. 398.

3 Smith D M, Screen J A, Deser C, Cohen J, Fyfe J C, *et al.*, The polar-amplification model Intercomparison project (PAMIP) contribution to CMIP6: Investigating the causes and consequences of polar amplification, *Geosci Model Dev*, 12 (2019) 1139–1164. https://doi.org/10.5194/gmd-12-1139-2019

4 Serreze M C & Barry R G, Processes and impacts of Arctic amplification: A research synthesis, *Global and Planetary Change*, 77 (1-2) (2011) 85-96. https://doi.org/10.1016/j.gloplacha.2011.03.004

5 Peixoto P, Abraham O, Curt C & Karl T, *Physics of Climate, Physics Today*, 45 (8) (1992) 67-67. https://doi.org/10.1063/1.2809772

6 Llovel W, Willis J K, Landerer F W & Fukumori I, Deep-ocean contribution to sea level and energy budget not detectable over the past decade, *Nature Climate Change*, 4 (11) (2014) 1031-1035. https://doi.org/10.1038/nclimate2387

7 Mayer M, Haimberger L & Balmaseda M A, On the Energy Exchange between Tropical Ocean Basins Related to ENSO, *J Clim*, 27 (17) (2014) 6393-6403. https://doi.org/10.1175/jcli-d-14-00123.1

8 Jackson C R & Apel J R (Eds), *Synthetic aperture radar: marine user's manual*, (NESDIS (National Environmental Satellite, Data, and Information Service)), 2004. https://repository.library.noaa.gov/view/noaa/1118

9 Martin T & Augstein E, Large-scale drift of Arctic Sea ice retrieved from passive microwave satellite data, *J Geophys Res Oceans*, 105 (C4) (2000) 8775-8788. https://doi.org/10.1029/1999jc900270

10 Yunhe Z, Liu A K & Long D G, Validation of sea ice motion from QuikSCAT with those from SSM/I and buoy, *IEEE Trans Geosci Remote Sens*, 40 (6) (2002) 1241-1246. https://doi.org/10.1109/tgrs.2002.800442

11 Kwok R, Seasonal ice area and volume production of the Arctic Ocean: November 1996 through April 1997, *J Geophys Res*, 107 (C10) (2002). https://doi.org/10.1029/2000jc000469

12 Laxon S, Peacock N & Smith D, High interannual variability of sea ice thickness in the Arctic region, *Nature*, 425 (6961) (2003) 947-950. https://doi.org/10.1038/nature02050

13 Årthun M, Eldevik T, Smedsrud L H, Skagseth Ø & Ingvaldsen R B, Quantifying the Influence of Atlantic Heat on Barents Sea Ice Variability and Retreat, *J Clim*, 25 (13) (2012) 4736-4743. https://doi.org/10.1175/jcli-d-11-00466.1

14 Onarheim I H & Årthun M, Toward an ice-free Barents Sea, *Geophy Res Lett*, 44 (16) (2017) 8387-8395. https://doi/10.1002/2017gl074304

15 Sigmond M, Reader M C, Flato G M, Merryfield W J & Tivy A, Skillful seasonal forecasts of Arctic sea ice retreat and advance dates in a dynamical forecast system, *Geophy Res Lett*, 43 (24) (2016) 12457–12465. https://doi/10.1002/2016gl071396

16 Onarheim I H, Eldevik T, Årthun M, Ingvaldsen R B & Smedsrud L H, Skillful prediction of Barents Sea ice cover, *Geophy Res Lett*, 42 (13) (2015) 5364-5371. https://doi/10.1002/2015gl064359

17 Smedsrud L H, Esau I, Ingvaldsen R B, Eldevik T, Haugan P M, *et al.*, The Role Of The Barents Sea In The Arctic Climate System, *Rev Geophys*, 51 (3) (2013) 415-449. https://doi/10.1002/rog.20017

18 Trenberth K E, Using Atmospheric Budgets as a Constraint on Surface Fluxes, *J Clim*, 10 (11) (1997) 2796-2809. https://doi/1175/1520-0442(1997)010<2796:uabaac>2.0.co;2

19 Nakamura N & Oort A H, Atmospheric heat budgets of the polar regions, *J Geophys Res*, 93 (D8) (1988) p. 9510. https://doi/10.1029/jd093id08p09510

20 Hersbach H, Bell B, Berrisford P, Biavati G, Horányi A, *et al.*, ERA5 monthly averaged data on single levels from 1940 to present, *Copernicus Climate Change Service (C3S) Climate Data Store (CDS)*, 2023. https://doi.org/10.24381/cds.f17050d7 (13/03/2022)

21 Schyberg H, Yang X, Køltzow M A Ø, Amstrup B, Bakketun Å, *et al.*, Arctic regional reanalysis on model levels from 1991 to present, *Copernicus Climate Change Service (C3S)Climate Data Store (CDS)*, 2020. https://doi.org/10.24381/cds.d29ad2c6 (13/03/2022)

22 Climate change: Ocean heat content, *NOAA Climate.gov science & information for a climate-smart nation*. https://www.climate.gov/news-features/understanding-climate/climate-change-ocean-heat-content (13/03/2022)

23 Kurtz N & Harbeck J, CryoSat-2 Level-4 Sea-ice Elevation, Freeboard, and Thickness, Version 1, [Sea-ice Thickness], *Boulder, Colorado USA, NASA National Snow and Ice Data Center Distributed Active Archive Center*, 2017. https://doi.org/10.5067/96JO0KIFDAS8

24 Kurtz N T, Galin N & Studinger M, An improved CryoSat-2 sea-ice freeboard retrieval algorithm through the use of waveform fitting, *The Cryosphere*, 8 (4) (2014) 1217–1237. https://doi.org/10.5194/tc-8-1217-2014

25 Warren S G, Rigor I G, Untersteiner N, Radionov V F, Bryazgin N N, *et al.*, Snow Depth on Arctic Sea-ice, *J Clim*, 12 (6) (1999) 1814–1829. https://doi.org/10.1175/1520-0442(1999)0122.0.co;2

26 Lindsay R & Schweiger A, Arctic Sea ice thickness loss determined using subsurface, aircraft, and satellite observations, *The Cryosphere*, 9 (1) (2015) 269-283. https://doi.org/10.5194/tc-9-269-2015

27 Serreze M C, Lynch A H & Clark M P, The Arctic frontal zone as seen in the NCEP–NCAR reanalysis, *J Clim*, 14 (7) (2001) 1550-1567. https://doi.org/10.1175/1520-0442(2001)014<1550:tafzas>2.0.co;2

28 Ebert E E & Curry J A, An intermediate one-dimensional thermodynamic sea ice model for investigating ice-atmosphere interactions, *J Geophys Res*, 98 (C6) (1993) p. 10085. https://doi.org/10.1029/93jc00656

29 Vasulkar A, Verlaan M & Slobbe C, *Towards the inclusion of sea-ice into a global tidal model*, 2021. https://doi.org/10.5194/egusphere-egu21-15359

30 Graham R M, Cohen L, Ritzhaupt N, Segger B & Graversen R G, Evaluation of six atmospheric Reanalyses over Arctic

Sea ice from winter to early summer, *J Clim*, 32 (14) (2019) 4121-4143. https://doi.org/10.1175/jcli-d-18-0643.1

31 Jakobson E, Vihma T, Palo T, Jakobson L, Keernik H, *et al.*, Validation of atmospheric reanalyses over the central Arctic Ocean, *Geophysical Research Letters*, (10) (2012), pp. 6. https://doi.org/10.1029/2012gl051591

32 Hersbach H, Bell B, Berrisford P, Dahlgren P, Horányi A, *et al.*, The ERA5 global reanalysis: Achieving a detailed record of the climate and weather for the past 70 years, (EGU General Assembly 2020, Online, 4–8 May 2020, EGU2020-10375), 2020. https://doi.org/10.5194/egusphere-egu2020-10375

33 Seo M, Kim H, Lee K, Seong N, Lee E, *et al.*, Characteristics of the reanalysis and satellite-based surface net radiation data in the Arctic, *J Sens*, (2020) 1-13. https://doi.org/10.1155/2020/8825870

34 Loeb N G, Wang H, Rose F G, Kato S, Smith W L, *et al.*, Decomposing Shortwave top-of-Atmosphere and surface radiative flux variations in terms of surface and atmospheric contributions, *J Clim*, 32 (16) (2019) 5003-5019. https://doi.org/10.1175/jcli-d-18-0826.1

35 Wang Y, Zhao X, Mamtimin A, Sayit H, Abulizi S, *et al.*, Evaluation of reanalysis datasets for solar radiation with in situ observations at a location over the Gobi region of Xinjiang, China, *Remote Sens*, 13 (21) (2021) p. 4191. https://doi.org/10.3390/rs13214191

36 Meyssignac B, Boyer T, Zhao Z, Hakuba M Z, Landerer F W, *et al.*, Measuring global ocean heat content to estimate the earth energy imbalance, *Front Mar Sci*, 6 (2019) 1-31. https://doi.org/10.3389/fmars.2019.00432

37 Sea ice concentrations from nimbus-7 smmr and dmspssm/I-ssmis passive microwave data, ver 1, (National Snow and Ice Data Center). https://nsidc.org/data/NSIDC-0051/versions/1

38 Kwok R, Arctic sea ice thickness, volume, and multiyear ice coverage: losses and coupled variability (1958–2018), *Environ Res Lett*, 13 (10) (2018) p. 105005. https://10.1088/1748-9326/aae3ec